Support information

Polyethyleneimine-Capped Copper Nanoclusters for Detection and Discrimination of 2,4,6-Trinitrotoluene and 2,4,6-Trinitrophenol

Haotian Wu,[1, 2, ‡] Guangfa Wang,[1, ‡] Zhenzhen Cai,[1, *] Dezhong Li,[1] Fangfang Xiao,[1, 2] Da Lei,[1] Zhuohua Dai,[1, 2] and Xincun Dou[1,2, *]

1. Xinjiang Key Laboratory of Explosives Safety Science, Xinjiang Technical Institute of Physics and Chemistry, Chinese Academy of Sciences, Urumqi 830000, China

2. Center of Materials Science and Optoelectronics Engineering, University of Chinese Academy of Sciences, Beijing 100049, China

‡ These authors contributed equally to this work.

* Corresponding authors. E-mail: caizz@ms.xjb.ac.cn (Zhenzhen Cai); xcdou@ms.xjb.ac.cn (Xincun Dou).

Optimization of the PEI-Cu NCs for TNT and TNP detection

Owing to long pair electrons on the N atom of amino, polyethyleneimine exhibits strong electron rich character in a wide range of pH, which can make polyethyleneimine capped copper nanoclusters (PEI-Cu NCs) donate electrons to the electron deficient molecules through p-electron donor-acceptor interaction, having the potential to chemically bind analyte molecule. Therefore, PEI anchored on the Cu NCs can easily bind hydrogen proton, which make PEI-Cu NCs exhibit pH-responsive properties. Firstly, the impact of the pH on the fluorescence of as-synthesis PEI-Cu NCs is investigated. It shows that the fluorescence intensity of PEI-Cu NCs is dramatically decreased with increasing the pH from 3-10, and there is no obvious emission peak shift within the investigated pH range (Fig. S3a). In basic medium, the donor character of PEI increases, causing the electrons transfer to PEI-Cu NCs and inhibiting the fluorescence emission. At low pH values, $-NH_2$ can easily combine hydrogen proton to form $-NH_3^+$, which makes PEI not able to transfer electrons because the oxidation process is inhibited. Afterwards, the sensitivity of TNT detection in different pH values based on PEI-Cu NCs is investigated. The fluorescence intensity at 500 nm is almost unchanged after the addition of TNT (Fig. S3b, $pH \leq 8$). While when $pH > 8$, with the increase of pH value, the fluorescence of PEI-Cu NCs is obviously quenched. It could be attributed to the deprotonation of the amino group of PEI to form Meisenheimer complex with TNT that can absorb the fluorescence of PEI-Cu NCs. On the contrary, the fluorescence of PEI-Cu NCs could be obviously quenched by TNP whatever in acid medium or alkaline medium (Fig. S3c), which imply that the mechanisms of fluorescence sensing toward TNT and TNP are different. We choose pH＝10 as the optimized detection condition because of considering the low original fluorescence intensity under strong alkaline conditions (pH＝11-14) and the potentially formed metal hydroxide precipitates. Moreover, the fluorescence quenching efficiency toward TNT and TNP is respectable under pH＝10, ensuring the consistent detection conditions.

It is important to point out that the different sensitivity of PEI-Cu NCs toward TNT and TNP in acid medium makes it possible a pH sensor accompanied with a TNT and TNP sensor. Time dependent fluorescence quenching of TNT and TNP is also investigated (Fig. S3d). A rapid equilibration of the reaction for TNT could be achieved within 5 min, and only within 3 min the system can reach about 85% of the final signal. The quenching efficiency is higher when TNP exists and a rapid equilibration of the reaction could be achieved within only 2 min.

Stern-Volmer equation and the triple signal-to-noise method

Stern-Volmer equation is used to describe the quenching efficiency as Equation:[1]

$$F_0/F = 1 + Ksv\,[Q] \qquad \text{(Equation S1)}$$

Here, F_0 and F respectively denote the fluorescence intensity before and after the detection, quenching constant is Ksv, and the molar concentration of the analyte is $[Q]$. The LOD of fluorescent and colorimetric detection is calculated by the following Equation:

$$\mathrm{LOD} = 3\sigma/k \qquad \text{(Equation S2)}$$

Here, σ denotes instrument standard deviation, and it is 1.24×10^{-4} in fluorescence spectrometer and 3.53×10^{-4} in UV-vis spectrophotometer, and k is the slope of the corresponding linear equation.

High Performance Liquid Chromatography analysis

In our applied Reversion Phase-HPLC method, an isocratic elution program was used by using 60% methanol + 40% H_2O (v/v) mixture as mobile phase at a flow rate of 1 mL min^{-1} and chromatograms recorded at 250 nm wavelength were used. The column was kept at 30 ℃ and the injection volume was 5 μL.

Cyclic voltametry analysis

Cyclic voltammetry tests are carried out using an electrochemical analyzer (CHI760D, CHI Instrument Inc.). The relating experiments are conducted using a conventional three-electrode system, in which a bare glassy carbon electrode is used as the working electrode, a platinum wire is used as the auxiliary electrode, and an Ag/AgCl electrode is used as the reference electrode. The first one-electron reduction potential onset (E_{ox}) is determined to be 0.97 eV (Fig. 4g). The ferrocene/ferrocenium

(Fc/Fc^+) redox potential is determined to be 0.53 eV (Fig. S6a). The highest occupied molecular orbitals (HOMO) energy of PEI-Cu NCs is determined to be -5.24 eV by the empirical formula Equation:[2]

$$HOMO = - [E_{ox} - E_{Fc/FC^+} + 4.8] \text{ eV} \quad \text{(Equation S3)}$$

Optical energy gap analysis

The optical energy gap of PEI-Cu NCs is analyzed by Tauc Plot method. The absorption spectrum of PEI-Cu NCs is obtained from ultraviolet-visible (UV-vis) spectrophotometer (U3900, Hitachi) (Fig. S6b). The relationship between the absorption spectrum and the optical energy gap could be achieved (Fig. 4f) according to the following formula Equation:[3]

$$(Ah\nu)^{1/n} = C\,(h\nu - E_g) \quad \text{(Equation S4)}$$

Here, A is the absorbance of PEI-Cu NCs, h is Planck constant, ν is photonic frequency of excitation light, n is a constant that determined by the intrinsic structure of the material, and it is 0.5 of PEI-Cu NCs resulting from its direct band gap. C is a constant. E_g is the absorption edge of PEI-Cu NCs in the UV-vis absorption spectrum. Thus, the optical energy gap of PEI-Cu NCs was determined to be 3.56 eV.

The lowest unoccupied molecular orbital (LUMO) of PEI-Cu NCs could be calculated by the following formula Equation:

$$E_{LUMO} = E_{HOMO} + E_g \quad \text{(Equation S5)}$$

Combining the HOMO and E_g of PEI-Cu NCs, the LUMO is determined to be -1.68 eV.

Calculation details

The quantum chemical analysis in this work is performed by the Gaussian 09C.[4] The geometric structure optimization is conducted through the density functional theory (DFT) with a PBE0[5] and Def2-tzvp[6] basis set, and then verifies that there is no virtual frequency in each geometric structure. Subsequently, the fluorescent property is carried out by a time-dependent density functional theory (TD-DFT) at optimized first excited state geometry with a PBE0/ Def2-tzvp level. The wave function analyses, such as analysis of excited states and the quantitative analyses of electrostatic potential (ESP),[7]

are conducted by using Multiwfn software.[8] Molecular configuration and orbital diagram is plotted by the VMD program.[9]

Procedure for vapor-phase detection of the TNT and TNP using Cu NCs-paper sensing chip

The appropriate analytes solid (0.0118 g for TNT and 0.0568 g for TNP) was placed in a tiny bottle, and then our paper sensing chip tied to a glass panel covered the mouth of the bottle. Finally, the equipment was placed in a drying oven (60 ℃, 3 hours) to yield corresponding TNT or TNP vapor.

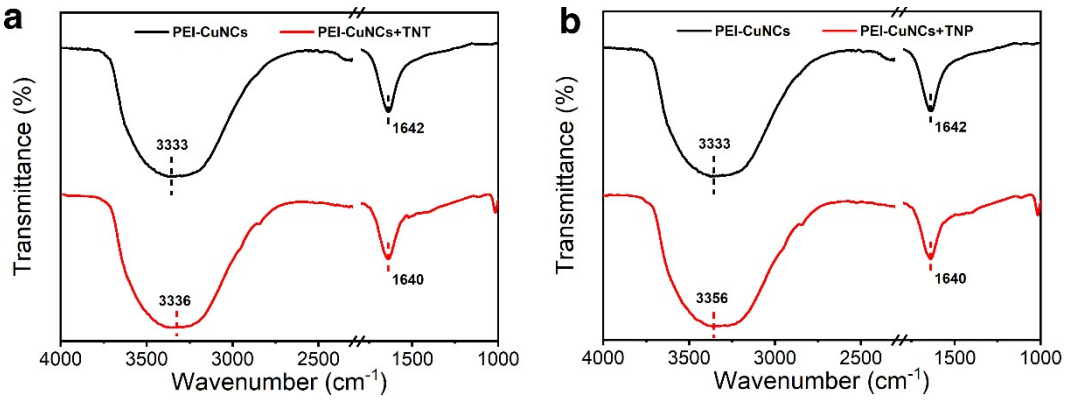

Fig. S1 ATR-FTIR spectra of PEI-Cu NCs before and after adding (a) TNT and (b) TNP.

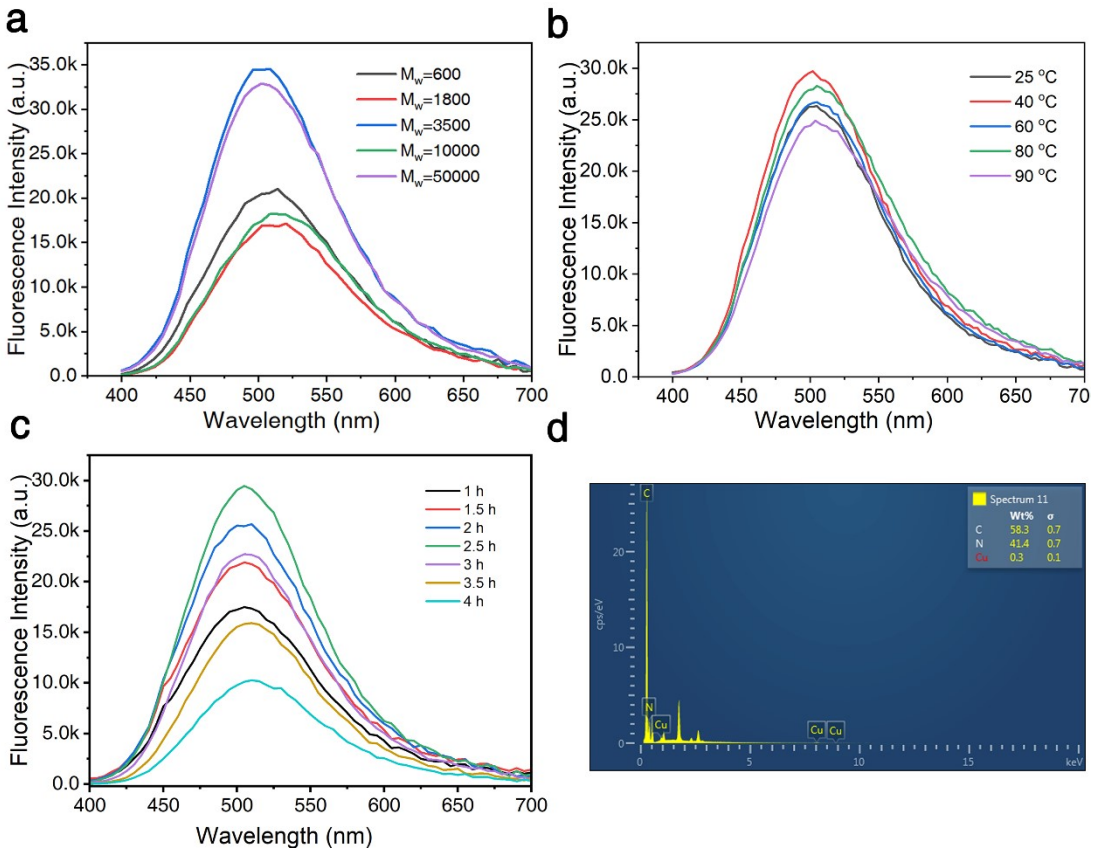

Fig. S2 (a) Emission spectra of PEI-Cu NCs with different molecular weight of PEI. (b) Emission spectra of PEI-Cu NCs with different synthesis temperature. (c) Emission spectra of PEI-Cu NCs with different synthesis time. (d) The quantitative analysis of C, N and Cu elements in PEI-Cu NCs by elemental mapping (λex= 390 nm; Slits: 2.0 nm; λem= 500 nm; Slits: 1.5 nm).

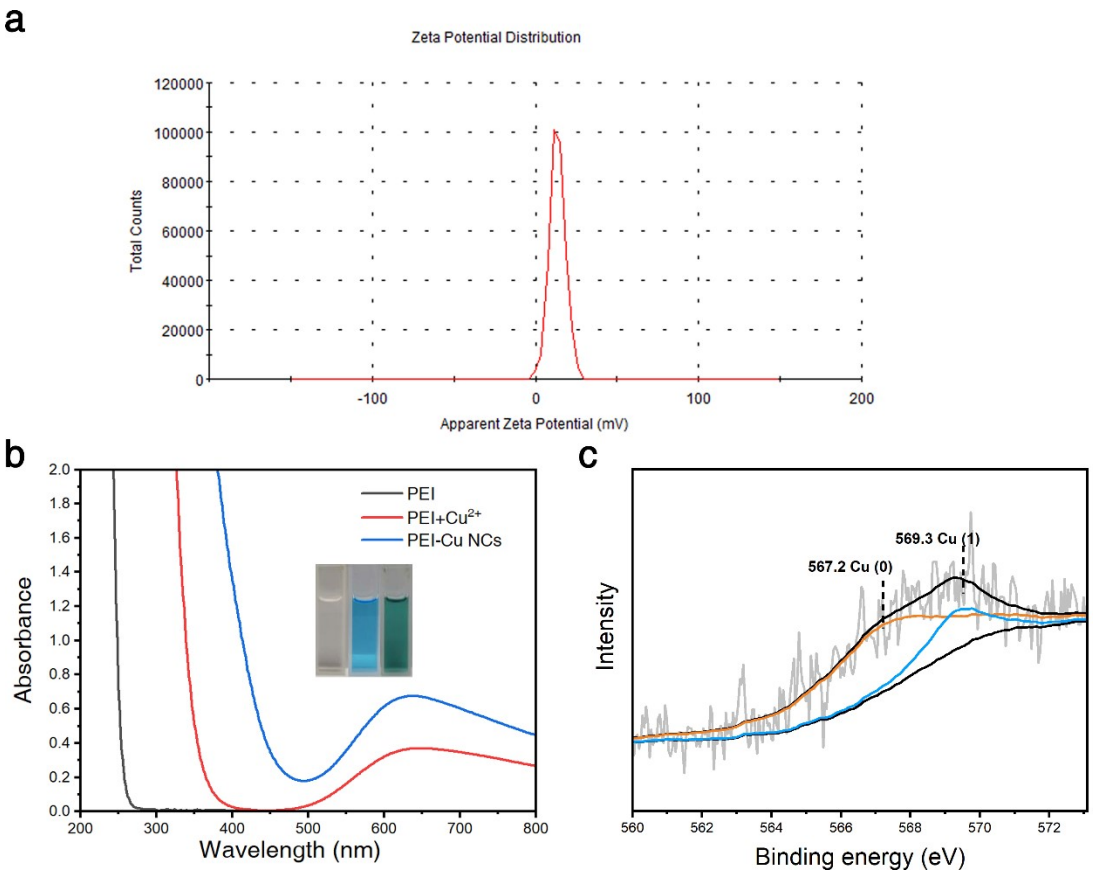

Fig. S3 (a) Zeta potential analysis of PEI-Cu NCs. (b) UV-vis absorption spectra of PEI, PEI-Cu^{2+} and PEI-Cu NCs, respectively. (c) X-ray induced auger electron spectra of PEI-Cu NCs.

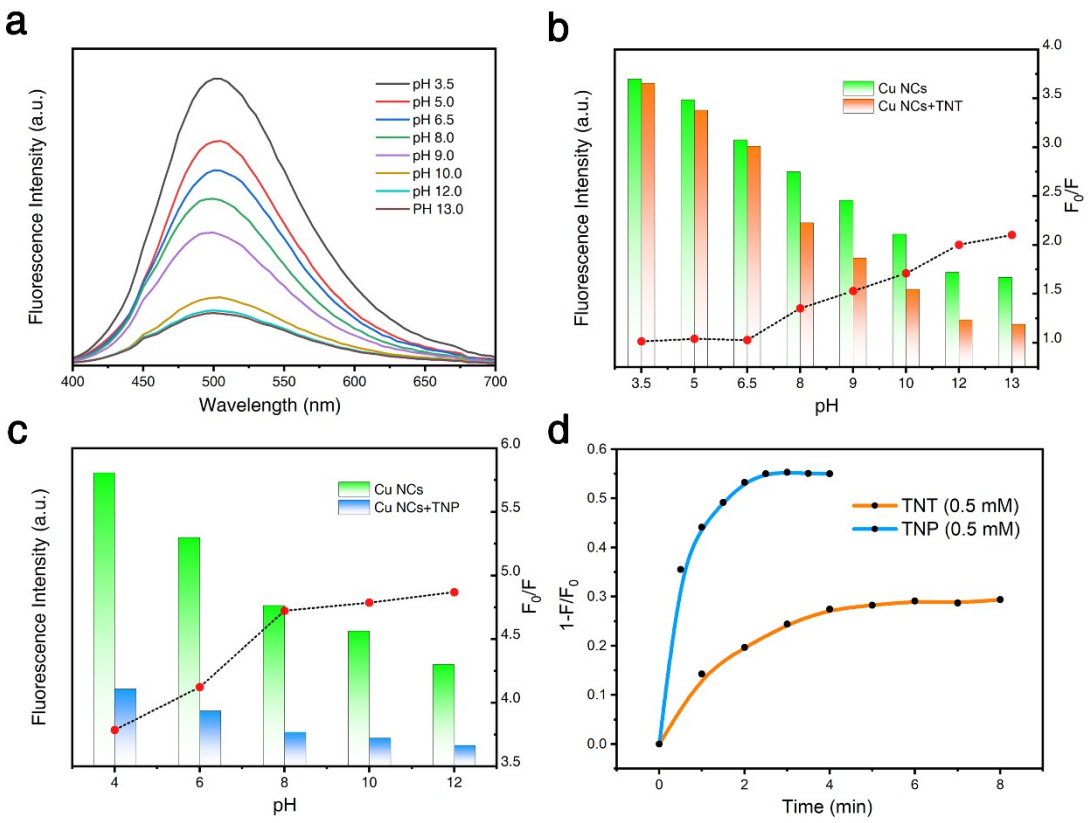

Fig. S4 (a) Effect of pH on the emission spectra of PEI-Cu NCs. (b) Effect of pH on the sensitivity of detecting TNT. (c) Effect of pH on the sensitivity of detecting TNP. (d) Time-dependent fluorescence changes of PEI-Cu NCs toward TNT and TNP. F_0 and F represent the fluorescence intensity in the absence and presence of target analytes, respectively.

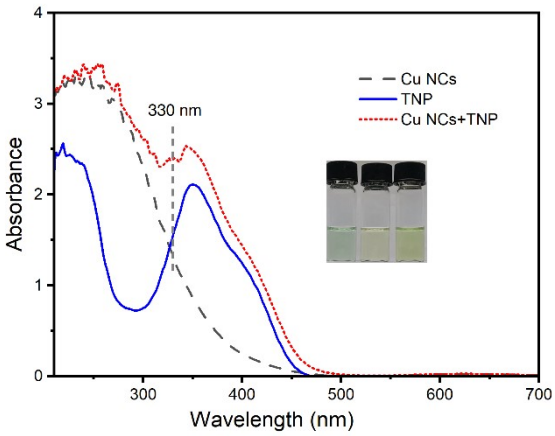

Fig. S5 UV-vis absorption spectra and photographs (inset) of the PEI-Cu NCs, TNP and their mixture.

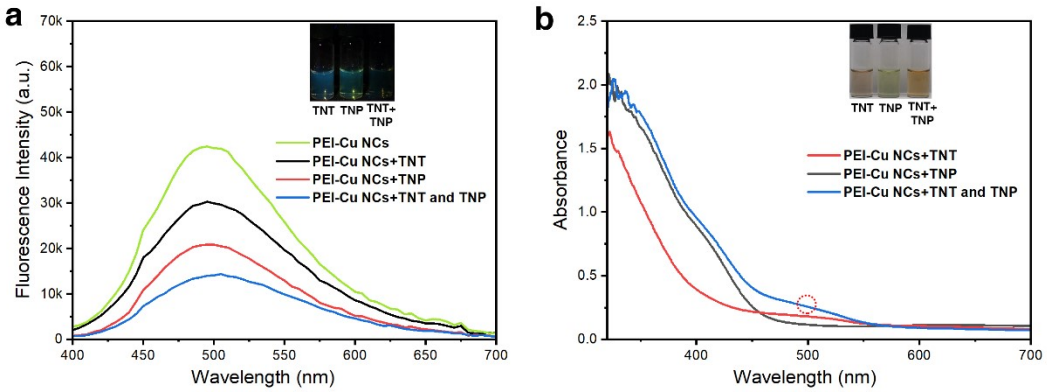

Fig. S6 (a) The emission spectra and photographs (inset) of PEI-Cu NCs after adding TNT, TNP and their mixture. (b) UV-vis absorption spectra and photographs (inset) of the PEI-Cu NCs after adding TNT, TNP and their mixture.

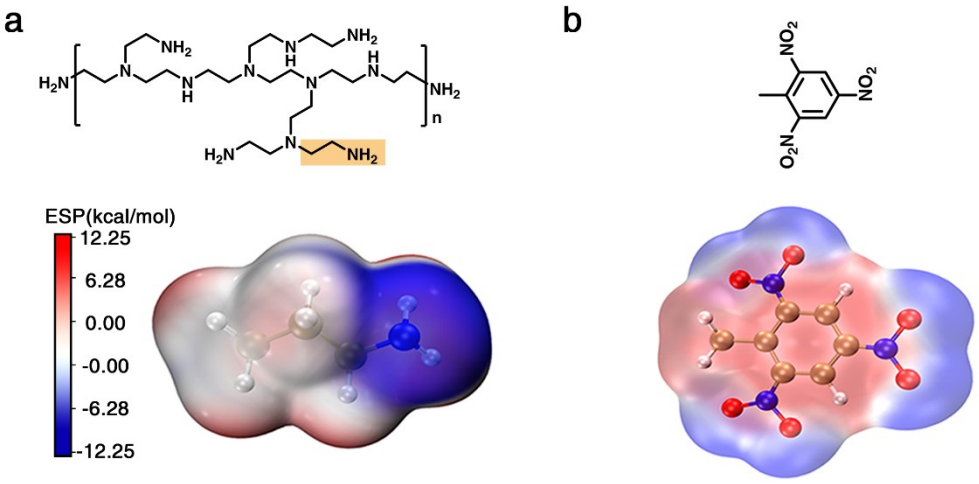

Fig. S7 The charge distribution simulation diagram of: (a) amino groups in PEI molecules; (b) TNT. (powered by Gaussian 09C, Multiwfn software and VMD program)

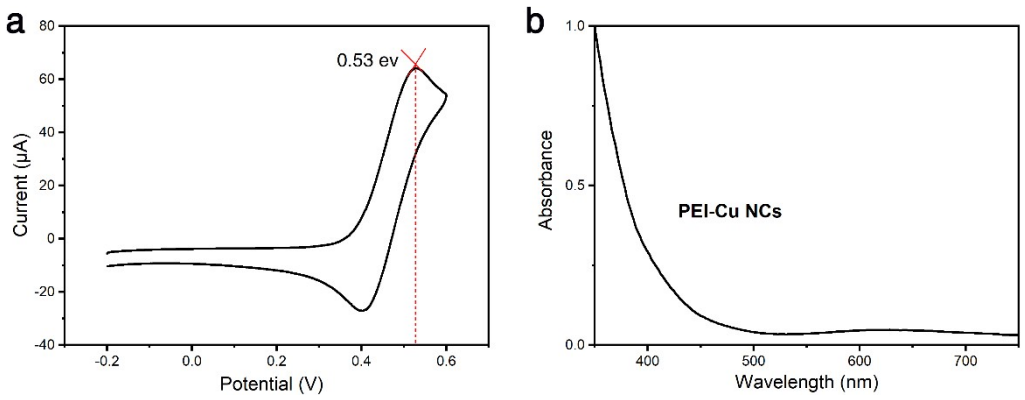

Fig. S8 (a) Cyclic voltammogram of ferrocene in 0.1 M THBP-DMF solution (10 mV/s, N_2 atmosphere). (b) UV-vis absorption spectrum of the PEI-Cu NCs.

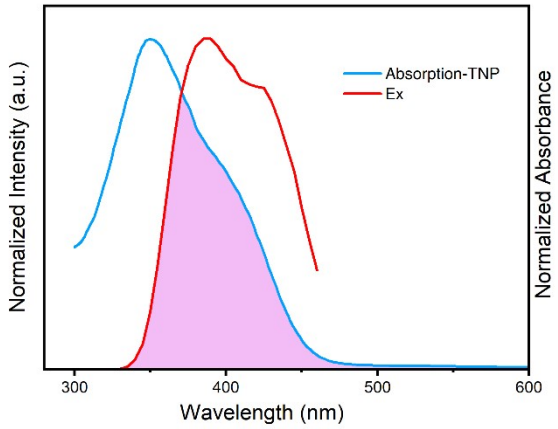

Fig. S9 The overlap of normalized excitation spectrum of PEI-Cu NCs and UV-vis absorption spectrum of TNP.

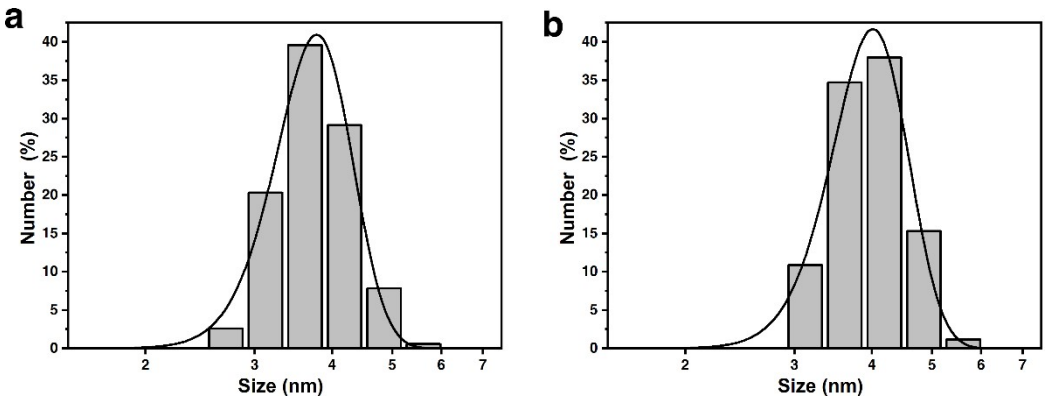

Fig. S10 DLS analysis of the size distribution of PEI-Cu NCs after the addition of (a) TNT and (b) TNP.

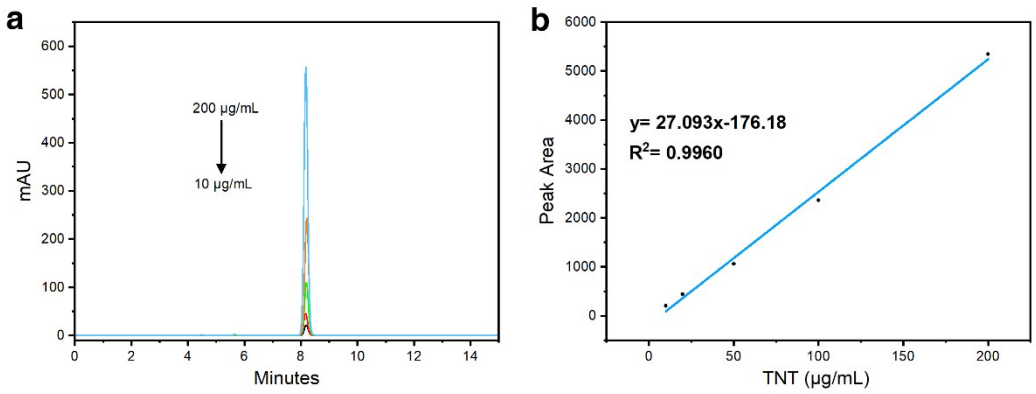

Fig. S11 (a) The HPLC chromatograms in the TNT concentration range (10 μg/mL-200 μg/mL). (b) The HPLC chromatograms working curve.

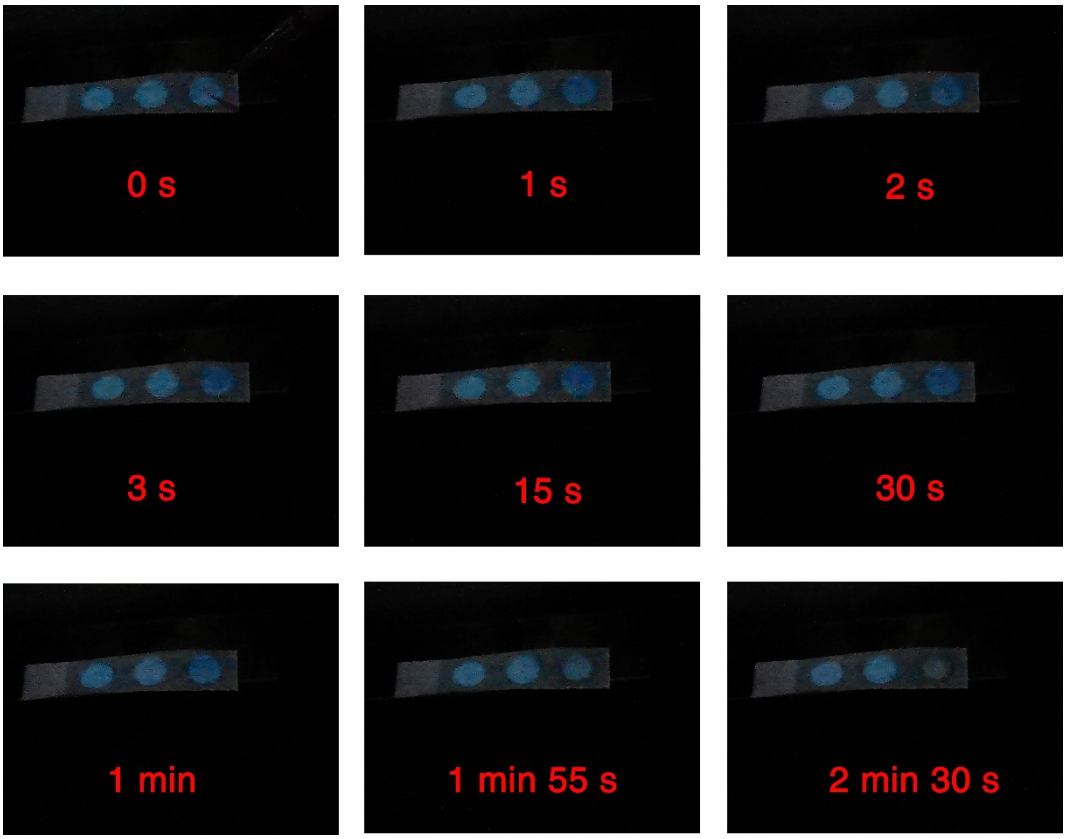

Fig. S12 Time-dependent photographs of Cu NCs-paper sensing chip for the fluorescence detection of TNT.

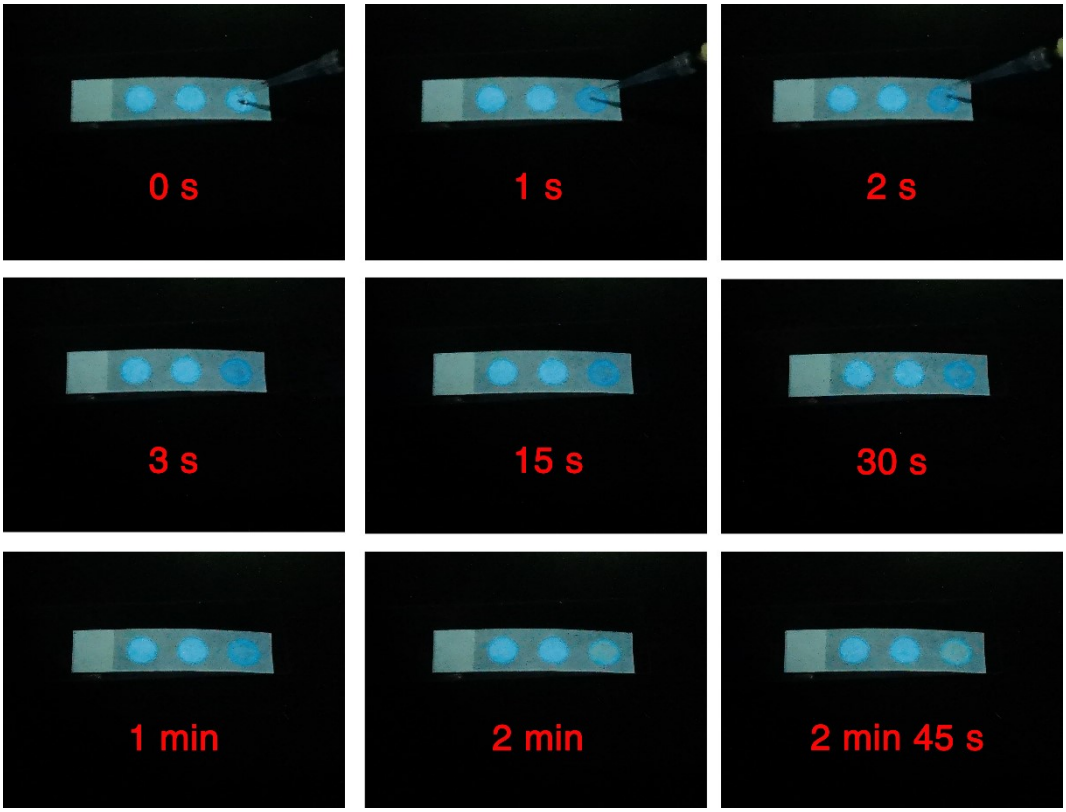

Fig. S13 Time-dependent photographs of Cu NCs-paper sensing chip for the fluorescence detection of TNP.

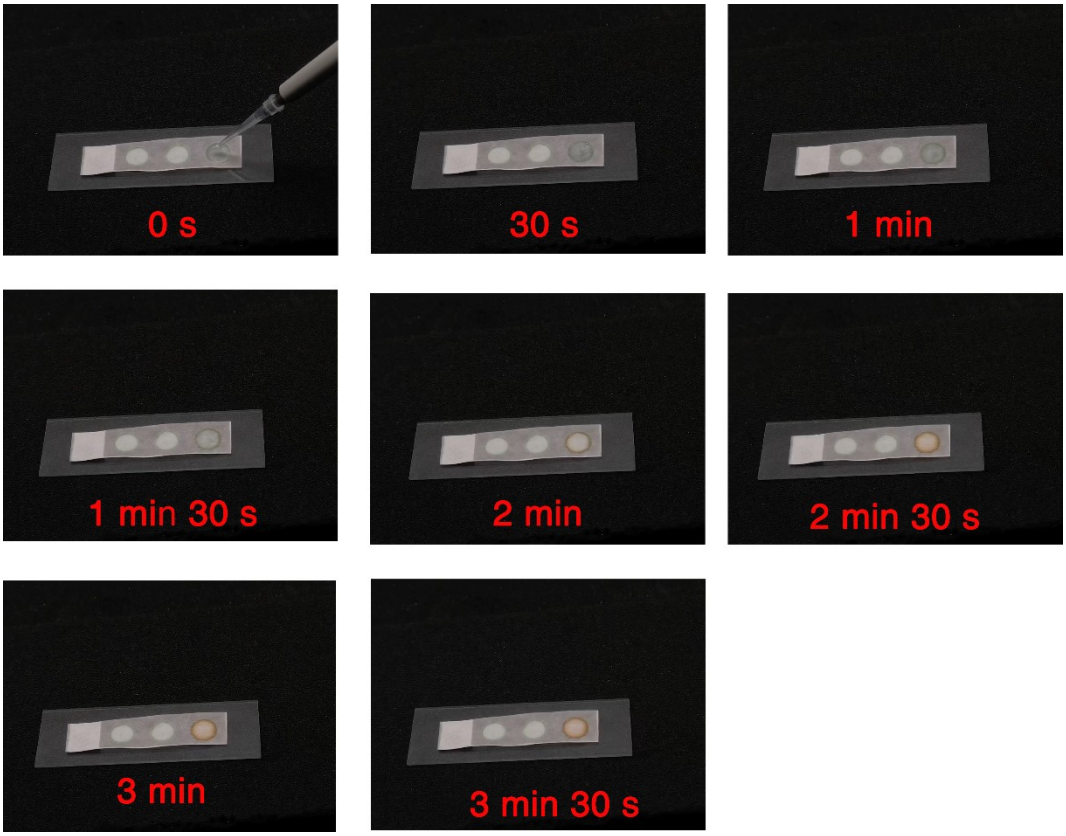

Fig. S14 Time-dependent photographs of Cu NCs-paper sensing chip for the colorimetric detection of TNT.

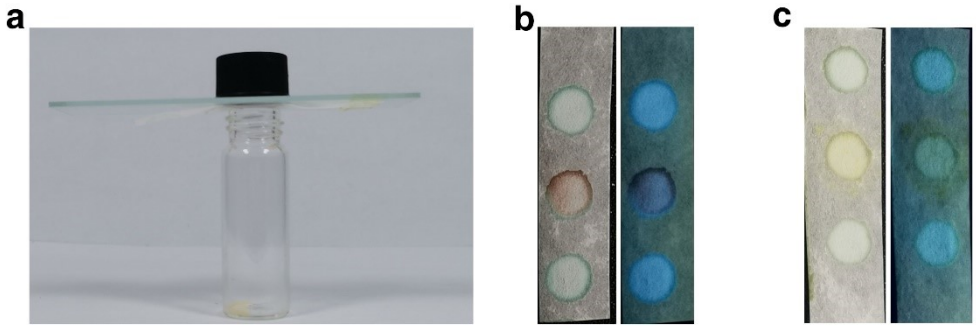

Fig. S15 (a) Practical equipment drawing of the vapor-phase detection for TNT or TNP. Vapor-phase detection of (b) TNT and (c) TNP using the Cu NCs-paper sensing chip under day light and 365 UV light.

Table S1. Comparison of different nanomaterials for determination of TNT or TNP.

Material	Analyte	LOD	Response mode	Discrimination	Ref.
N-rich carbon nanodots	TNT	Fluorescent 1 nM Electrochemical 1nM	Fluorescent and Electrochemical	NO	10
PEI-CuNC	TNT	Fluorescence 14 pM Colorimetric 0.05 nM	Fluorescent and Colorimetric	NO	11
NH_2–Cu-MOF	TNP	80 nM	Fluorescent	NO	12
CuNCs@PVP	TNP	0.391 μM	Fluorescent	NO	13
Cys–CuNCs	TNP	0.19 μM	Fluorescent	NO	14
PVP-CuNCs	TNP	81.44 pM	Fluorescent	NO	15
Cu NCs	TNP	0.98 μM	Fluorescent	NO	16
PEI-G PNPs	TNP	26 nM	Fluorescent	NO	17
Carbon dot	TNP	0.68 μM	Fluorescent	NO	18
PEI-C-dots	TNT	93.1 μg/L	Fluorescent	NO	19
AuNCs/ZIF-8	TNT	5 nM	Fluorescent	NO	20
Cu NC/ZIF-8	TNT	8.5 μM	Fluorescent	NO	21
Au@Ag NPs	TNT	0.35 μg/mL	Colorimetric	NO	22
DACH/TGA@ AuNPs	TNT and tetryl	1.76 pM (TNT) 1.74 pM (tetryl)	Colorimetric	NO	23
BSA Au-NCs	TNT and 4-NP	10 nM (TNT) 1 nM (4-NP)	Fluorescent	NO	24
PEI-Cu NCs	**TNT and TNP**	**Fluorescent (TNT) 26.57 nM; (TNP) 12.82 nM** **Colorimetric (TNT) 0.39 μM**	**Fluorescent and Colorimetric**	**Yes**	**This work**

Table S2. Fluorescence lifetime of PEI-Cu NCs before and after the presence of TNT or TNP. Pulsed excitation of 405 nm is used to measure the decay profile.

Samples	τ_1 (ns) (f_1)	τ_2 (ns) (f_2)	τ_3 (ns) (f_3)	τave (ns)	χ^2
PEI-Cu NCs	0.44 (8.23)	2.39 (65.17)	7.84 (26.60)	3.68	1.166
PEI-Cu NCs + TNT	0.37 (22.95)	2.27 (50.58)	7.30 (26.47)	3.16	1.087
PEI-Cu NCs + TNP	0.46 (22.61)	2.43 (51.73)	7.38 (25.66)	3.25	1.144

Table S3. The binding energy between PEI and some nitroaromatic compounds

Targets	Binding energy (kcal/mol)
PEI-TNP	**-9.09**
PEI-DNB	-8.55
PEI-NA	-9.51
PEI-NB	-4.35
PEI-NBZA	-5.80
PEI-RDX	-2.67
PEI-Toluene	-4.61
PEI-DNT	-7.85

Table S4 Detection of TNT and TNP in tap water samples with our

proposed method

Sample	Added (μM)	Detected (μM)	Recovery (%)	RSD (n =3%)
TNT in tap water	0	—	—	—
	75	74.95	99.93	0.90
	30	31.50	99.86	5.15
	12.5	12.91	103.30	1.99
TNP in tap water	0	—	—	—
	50	47.06	94.12	2.53
	25	24.20	96.80	3.04
	12.5	12.65	101.18	5.69

Supporting Videos (1-3)

Video S1: Fluorescent detection of TNT with Cu NCs-paper sensing chip (triple speed).

Video S2: Fluorescent detection of TNP with Cu NCs-paper sensing chip (triple speed).

Video S3: Colorimetric detection of TNT with Cu NCs-paper sensing chip (triple speed).

References

1. J. R. Lakowicz, *Principles of fluorescence spectroscopy*, Springer, New York, 3rd edn., 2006.
2. C. M. Cardona, W. Li, A. E. Kaifer, D. Stockdale and G. C. Bazan, *Adv. Mater.*, 2011, **23**, 2367-2371.
3. F. Qu, X. Li, X. Lv, J. You and W. Han, *J. Mater. Sci.*, 2019, **54**, 3144-3155.
4. M. J. Frisch, G. W. Trucks, H. B. Schlegel, G. E. Scuseria, M. A. Robb, J. R. Cheeseman, G. Scalmani, V. Barone, G. A. Petersson, H. Nakatsuji, X. Li, M. Caricato, A. V. Marenich, J. Bloino, B. G. Janesko, R. Gomperts, B. Mennucci, H. P. Hratchian, J. V. Ortiz, A. F. Izmaylov, J. L. Sonnenberg, Williams, F. Ding, F. Lipparini, F. Egidi, J. Goings, B. Peng, A. Petrone, T. Henderson, D. Ranasinghe, V. G. Zakrzewski, J. Gao, N. Rega, G. Zheng, W. Liang, M. Hada, M. Ehara, K. Toyota, R. Fukuda, J. Hasegawa, M. Ishida, T. Nakajima, Y. Honda, O. Kitao, H. Nakai, T. Vreven, K. Throssell, J. A. Montgomery Jr., J. E. Peralta, F. Ogliaro, M. J. Bearpark, J. J. Heyd, E. N. Brothers, K. N. Kudin, V. N. Staroverov, T. A. Keith, R. Kobayashi, J. Normand, K. Raghavachari, A. P. Rendell, J. C. Burant, S. S. Iyengar, J. Tomasi, M. Cossi, J. M. Millam, M. Klene, C. Adamo, R. Cammi, J. W. Ochterski, R. L. Martin, K. Morokuma, O. Farkas, J. B. Foresman and D. J. Fox, *Journal*, 2016.
5. C. Adamo and V. Barone, *J. Chem. Phys.*, 1999, **110**, 6158-6170.
6. A. Schäfer, H. Horn and R. Ahlrichs, *J. Chem. Phys.*, 1992, **97**, 2571-2577.
7. T. Lu and F. Chen, *J. Mol. Graph. Model.*, 2012, **38**, 314-323.
8. T. Lu and F. Chen, *J. Comput. Chem.*, 2012, **33**, 580-592.
9. W. Humphrey, A. Dalke and K. Schulten, *J. Mol. Graph.*, 1996, **14**, 33-38.
10. L. Zhang, Y. Han, J. Zhu, Y. Zhai and S. Dong, *Anal. Chem.*, 2015, **87**, 2033-2036.
11. R. S. Aparna, J. S. Anjali Devi, P. Sachidanandan and S. George, *Sens. Actuators, B*, 2018, **254**, 811-819.
12. J. Chen, Q. Zhang, J. Dong, F. Xu and S. Li, *Anal. Methods*, 2021, **13**, 5328-5334.
13. Y. Li, L. Feng, W. Yan, I. Hussain, L. Su and B. Tan, *Nanoscale*, 2019, **11**, 1286-1294.
14. K. Shanmugaraj and S. A. John, *New J. Chem.*, 2018, **42**, 7223-7229.

15. R. Rajamanikandan and M. Ilanchelian, *ACS Omega*, 2018, **3**, 18251-18257.
16. W. J. Zhang, S. G. Liu, L. Han, Y. Ling, L. L. Liao, S. Mo, H. Q. Luo and N. B. Li, *Anal. Methods*, 2018, **10**, 4251-4256.
17. S. G. Liu, D. Luo, N. Li, W. Zhang, J. L. Lei, N. B. Li and H. Q. Luo, *ACS Appl. Mater. Interfaces*, 2016, **8**, 21700-21709.
18. A. Kathiravan, A. Gowri, V. Srinivasan, T. A. Smith, M. Ashokkumar and M. Asha Jhonsi, *Analyst*, 2020, **145**, 4532-4539.
19. F. B. Şen, N. Beğiç, M. Bener and R. Apak, *Spectrochim. Acta, Part A*, 2022, **271**, 120884.
20. Y. Zhao, M. Pan, F. Liu, Y. Liu, P. Dong, J. Feng, T. Shi and X. Liu, *Anal. Chim. Acta*, 2020, **1106**, 133-138.
21. Z. Wang, R. Chen, Y. Xiong, K. Cepe, J. Schneider, R. Zboril, C.-S. Lee and A. L. Rogach, *Part. Part. Syst. Char.*, 2017, **34**, 1700029.
22. A. Arshad, H. Wang, X. Bai, R. Jiang, S. Xu and L. Wang, *Spectrochim. Acta, Part A*, 2019, **206**, 16-22.
23. N. Ular, A. Üzer, S. Durmazel, E. Erçağ and R. Apak, *ACS Sensors*, 2018, **3**, 2335-2342.
24. X. Yang, J. Wang, D. Su, Q. Xia, F. Chai, C. Wang and F. Qu, *Dalton Trans.*, 2014, **43**, 10057-10063.